2026 IEEE/SICE International Symposium on System Integration (SII)
January 11-14, 2026. Cancún, México

Salient Behavior Extraction in Construction Machinery Operation Using Motion Propagation Forces

Ryo Sumiyama, Takashi Kusaka, Hironori Gunji, Yuichi Kurita,
Fumiya Sakamoto, Masaru Ito, Yusuke Kamimura and Takayuki Tanaka

***Abstract*— This study proposes a vibration-feedback method to enhance kinesthetic perception while reducing lumbar load during the teleoperation of construction machinery. The angular acceleration of the operator's seat is dynamically estimated from joint torques, and salient vibration components are extracted from their decomposed terms. Using the partial Lagrangian method and the concept of motion-propagation force, we isolate the torque component at the base joint induced by the motion of a specific link and analyze its contribution to seat angular acceleration via wavelet transforms. Excavation experiments demonstrate that the extracted component significantly influences seat angular acceleration, suggesting that selective vibration feedback can preserve operational feel while alleviating operator workload.**

I. INTRODUCTION

In recent years, the construction industry has faced severe labor shortages and harsh working conditions, prompting the adoption of teleoperation technologies as a potential solution. Teleoperation enables operators to control construction machinery remotely while reproducing real-time visual and dynamic feedback, providing a sense of presence comparable to on-site operation. For instance, K-DIVE® (developed by Kobelco Construction Machinery Co.) captures seat inclination and vibration data from sensors on the machine and reproduces them in the remote cockpit, enhancing operational realism.

However, reproducing seat motion also transmits mechanical load to the operator's lower back, potentially offsetting the benefits of enhanced kinesthetic perception. This highlights the need for a remote operational environment that can maintain operational feel while minimizing physical strain.

Previous studies have addressed kinesthetic feedback by reflecting forces on joysticks[1][2] or by augmenting visual cues[3]. In this study, we propose a novel approach: selectively controlling seat angular acceleration based on dynamic torque analysis to preserve perception and reduce unnecessary vibration.

Specifically, we compute the operator's seat angular acceleration from the machine's joint torques, decompose these torques using the partial Lagrangian method[4] and motion-propagation force analysis[5], and identify the torque components that most affect haptic sensation. These model-based decomposition techniques allow us to isolate physically interpretable vibration sources, enabling targeted reproduction that balances immersion and comfort

Unlike conventional frequency-based filtering[6], our method links vibration feedback directly to structural motion components, supporting more ergonomic teleoperation. We validate the proposed approach through wavelet-based analysis[7] and full-scale excavation experiments.

The remainder of this paper is organized as follows. Section II presents the proposed method. Section III describes the experimental setup. Section IV presents the results, Section V provides discussion, and Section VI concludes the paper.

II. PROPOSED METHOD

A. Torque Computation via the Partial-Lagrangian Method

For an n-degree-of-freedom (DoF) serial-link manipulator subject to an external force at the end-effector, the joint-torque vector $\boldsymbol{\tau}$ is obtained as follows. First, the partial-Lagrangian method is employed to compute, for each joint, the torque generated by its voluntary motion together with the corresponding partial torque. In Lagrange's equations of motion, the Lagrangian $\mathcal{L}$ is defined from the kinetic energy K and the potential energy P as

$$\mathcal{L} = K - P \tag{1}$$

In the Lagrangian formulation, the equations of motion are obtained as

$$\frac{d}{dt}\left(\frac{\partial \mathcal{L}}{\partial \dot{q}_k}\right) - \frac{\partial \mathcal{L}}{\partial q_k} = \tau_k \tag{2}$$

Here, q_k and τ_k denote the k-th generalized coordinate and generalized force, respectively.

For compact notation, we introduce the differential operator $\mathcal{D}_k$

$$\mathcal{D}_k = \frac{d}{dt}\left(\frac{\partial}{\partial \dot{q}_k}\right) - \frac{\partial}{\partial q_k} \tag{3}$$

Using the energy-distribution method, Eq. (1) can be rewritten for an n-link system as

$$\mathcal{L} = \sum_{i=1}^{n} K_i - \sum_{i=1}^{n} P_i = \sum_{i=1}^{n} (K_i - P_i) = \sum_{i=1}^{n} \mathcal{L}_i \tag{4}$$

*This work was not supported by any organization.

[1]Ryo Sumiyama, Takashi Kusaka, Hironori Gunji, and Takayuki Tanaka are with Hokkaido University, Japan.

[2]Yuichi Kurita and Fumiya Sakamoto is with Hiroshima University, Japan.

[3]Masaru Ito and Yusuke Kamimura are with Kobelco Construction Machinery Co., Ltd., Japan.

Applying the operator $\mathcal{D}_k$ to the partial Lagrangian $\mathcal{L}_i$ associated with link i yields the partial torque τ_{ki} at joint k, as expressed in Eq. (5).

$$D_k\mathcal{L} = D_k \sum_{i=1}^{n} \mathcal{L}_i = \sum_{i=1}^{n} D_k\mathcal{L}_i = \sum_{i=1}^{n} \tau_{ki} \tag{5}$$

Because $\mathcal{L}_i$ contains q_k only when $i \geq k$, the partial torque has the property

$$D_k\mathcal{L}_i = \begin{cases} \tau_{ki} & \text{if } i \geq k \\ 0 & \text{if } i < k \end{cases} \tag{6}$$

TABLE I summarizes these relationships. Through this partial-Lagrangian approach, we obtain both the voluntary (self-induced) joint torque and its constituent partial torques for the manipulator.

TABLE I: Relationship between partial Lagrangian and Lagrangian methods.

	$\mathcal{L}_1$	$\mathcal{L}_2$	$\mathcal{L}_3$	$\cdots$	$\mathcal{L}_i$	$\cdots \mathcal{L}_n$	$\sum$	$\mathcal{L}$
D_1	τ_{11}	τ_{12}	τ_{13}	$\cdots$	τ_{1i}	$\cdots \tau_{1n}$	$\rightarrow$	τ_1
D_2	0	τ_{22}	τ_{23}	$\cdots$	τ_{2i}	$\cdots \tau_{2n}$	$\rightarrow$	τ_2
D_3	0	0	τ_{33}	$\cdots$	τ_{3i}	$\cdots \tau_{3n}$	$\rightarrow$	τ_3
$\vdots$	$\vdots$	$\vdots$	$\vdots$	$\ddots$	$\vdots$	$\ddots$	$\vdots$	$\vdots$
D_k	0	0	0	$\cdots$	τ_{ki}	$\cdots \tau_{kn}$	$\rightarrow$	τ_k
$\vdots$	$\vdots$	$\vdots$	$\vdots$	$\ddots$	$\vdots$	$\ddots$	$\vdots$	$\vdots$
D_n	0	0	0	$\cdots$	0	τ_{nm}	$\rightarrow$	τ_n

Next, we calculate the torques resulting from external forces. Among the forces acting on the end-effector, the horizontal component in the sagittal plane (as seen by the operator) is denoted Fx, and the vertical component is denoted Fy The end-effector force vector $\boldsymbol{F}$ is thus defined as in Eq. (7).

$$\boldsymbol{F} = [F_x, F_y]^T \tag{7}$$

Using forward kinematics, the end-effector position of link i is obtained as r_i and the position vector $\boldsymbol{r}$ is defined accordingly (8).

$$\boldsymbol{r} = [r_1, r_2, \ldots, r_n]^T \tag{8}$$

Here, let θ_i denote the angle of the i-th joint of the manipulator, and define the joint-variable vector $\boldsymbol{\theta}$ as in Eq. (9).

$$\boldsymbol{\theta} = [\theta_1, \theta_2, \ldots, \theta_n]^T \tag{9}$$

The relationship between $\boldsymbol{r}$ and $\boldsymbol{\theta}$ is generally expressed by (10).

$$\boldsymbol{r} = \boldsymbol{f}(\boldsymbol{\theta}) \tag{10}$$

These expressions allow the Jacobian matrix $\boldsymbol{J}$ to be derived as shown in (11).

$$\boldsymbol{J} = \frac{\partial \boldsymbol{f}(\boldsymbol{\theta})}{\partial \boldsymbol{\theta}^T} \tag{11}$$

Let τ_i denote the torque acting on the i-th joint, and τ_{ij} the partial torque at joint i attributable to link j. Defining the joint-torque vector $\boldsymbol{\tau}$ as in the equation, the relationships can be expressed as Eqs. (12) and (13).

$$\boldsymbol{\tau} = [\tau_1, \tau_2, \ldots, \tau_n]^T \tag{12}$$

$$= \begin{bmatrix} \tau_{11} & \tau_{12} & \cdots & \tau_{1n} \\ 0 & \tau_{22} & \cdots & \tau_{2n} \\ \vdots & \vdots & \ddots & \vdots \\ 0 & 0 & \cdots & \tau_{nn} \end{bmatrix} \begin{bmatrix} 1 \\ 1 \\ \vdots \\ 1 \end{bmatrix} + \boldsymbol{J}^T\boldsymbol{F} \tag{13}$$

Here, $\boldsymbol{J}^T\boldsymbol{F}$ is taken as the external-force term.

B. Salient Behavior Separation

Next, we extract as the salient behaviors the motion-propagation forces—the forces transmitted to other joints as the joint motions of an n-DoF serial-link manipulator propagate through each link. The quantity $\tau_{ij}^p\left(\theta_k^{(m)}\right)$ is defined, as in Eqs. (14) and (15), as the torque applied to joint i due to the motion of link j.

$$\tau_{ij}^p\left(\theta_k^{(m)}\right) = \frac{\partial \tau_{ij}}{\partial \theta_k^{(m)}} \theta_k^{(m)} \tag{14}$$

$$\theta_i^{(2)} = \ddot{\theta}_l \tag{15}$$

Here, $\theta_i^{(m)}$ denotes the m-th time derivative of θ_i.
The partial torque is then expressed as in Eq. (16)

$$\tau_{ij} = \boldsymbol{M}_{ij}\ddot{\boldsymbol{\theta}} + V_{ij}(\dot{\boldsymbol{\theta}}, \boldsymbol{\theta}) + G_{ij}(\boldsymbol{\theta}) \tag{16}$$

where $M_{ij} \in \mathbb{R}^{1\times n}$ is the inertia matrix, $V_{ij}(\dot{\boldsymbol{\theta}}, \boldsymbol{\theta})$ is a function of the velocity-squared term, and $G_{ij}(\boldsymbol{\theta})$ is a function of the gravity effect. Next, the partial torque can be expressed in terms of the auto-derivative concept, as shown in Equations (17)–(19).

$$\tau_{ij} = \sum_{s=1}^{j} \frac{\partial \tau_{ij}}{\partial \ddot{\theta}_s}\ddot{\theta}_s + \frac{1}{2}\sum_{s=1}^{j} \frac{\partial \tau_{ij}}{\partial \dot{\theta}_s}\dot{\theta}_s + \sum_{s=1}^{j} \frac{\partial \tau_{ij}}{\partial \dot{\theta}_s^2}\dot{\theta}_s^2 + G_{ij}(\boldsymbol{\theta}) \tag{17}$$

$$\simeq \sum_{s=1}^{j} \frac{\partial \tau_{ij}}{\partial \ddot{\theta}_s}\ddot{\theta}_s + \frac{1}{2}\sum_{s=1}^{j} \frac{\partial \tau_{ij}}{\partial \dot{\theta}_s}\dot{\theta}_s + \sum_{s=1}^{j} \frac{\partial \tau_{ij}}{\partial \dot{\theta}_s^2}\dot{\theta}_s^2 + \sum_{s=1}^{j} \frac{\partial \tau_{ij}}{\partial \theta_s}\theta_s \tag{18}$$

$$= \sum_{b=0}^{2} \boldsymbol{c}_b \cdot \boldsymbol{\theta}^{(b)} \tag{19}$$

$\mathbf{c}_2 \in \mathbb{R}^{1\times n}$ is the coefficient matrix (row vector) for acceleration, $\mathbf{c}_1 \in \mathbb{R}^{1\times n}$ for velocity, and $\mathbf{c}_0 \in \mathbb{R}^{1\times n}$ for position. Consequently, the partial torque τ_{ij} is the torque generated at joint i by the motion of link j expressed in the world coordinate frame. Therefore, by evaluating Eq. (14), one can isolate from the partial torque only the contribution due to the link's joint motion and derive it as the motion-propagation torque, yielding Eqs. (20) and (21).

$$\tau_{ij}^{p}(\theta_k^{(m)}) = \frac{\partial}{\partial \theta_k^{(m)}} \left(\sum_{b=0}^{2} \boldsymbol{c}_b \cdot \boldsymbol{\theta}^{(b)} \right) \theta_k^{(m)} \tag{20}$$

$$= \sum_{b=0}^{2} \frac{\partial (\boldsymbol{c}_b \cdot \boldsymbol{\theta}^{(b)})}{\partial \theta_k^{(m)}} \theta_k^{(m)} \tag{21}$$

Here, all terms other than the one of interest, $\theta_1^{(m)}$ for $m \neq b$, become zero and cancel out. Consequently, the target term $\theta_1^{(m)}$ with $m = b$ can be systematically extracted, as indicated in Eqs. (22) and (23).

$$\tau_{ij}^{p}(\theta_k^{(m)}) = \left(\frac{\partial (\boldsymbol{c}_b \cdot \boldsymbol{\theta}^{(b)})}{\partial \theta_k^{(m)}} \bigg|_{b=m} \right) \theta_k^{(m)} \tag{22}$$

$$= c_{mk}\, \theta_k^{(m)} \tag{23}$$

From these relations, the partial torque can be expressed as in Eqs. (24)-(28).

$$\tau_{ij} \simeq \sum_{b=0}^{2} \boldsymbol{c}_b \cdot \boldsymbol{\theta}^{(b)} = \sum_{b=0}^{2} \left(\sum_{s=1}^{j} c_{bs} \theta_s^{(b)} \right) \tag{24}$$

$$= \sum_{s=1}^{i} \left(\sum_{b=0}^{2} c_{bs} \theta_s^{(b)} \right) \tag{25}$$

$$= \sum_{s=1}^{j} \left(\begin{bmatrix} c_{0s} & c_{1s} & c_{2s} \end{bmatrix} \begin{bmatrix} 1 & 0 & 0 \\ 0 & 1 & 0 \\ 0 & 0 & 1 \end{bmatrix} \begin{bmatrix} \theta_s \\ \dot{\theta}_s \\ \ddot{\theta}_s \end{bmatrix} \right) \tag{26}$$

$$= \sum_{s=1}^{j} \left(\begin{bmatrix} c_{0s} & c_{1s} & c_{2s} \end{bmatrix} \sum_{m=0}^{2} \boldsymbol{M}_{(m)} \begin{bmatrix} \theta_s \\ \dot{\theta}_s \\ \ddot{\theta}_s \end{bmatrix} \right) \tag{27}$$

$$\boldsymbol{M}_{(m)} = \begin{bmatrix} \delta(m-0) & 0 & 0 \\ 0 & \delta(m-1) & 0 \\ 0 & 0 & \delta(m-2) \end{bmatrix} \tag{28}$$

Here, $\delta(x)$ denotes the Kronecker delta, with $\delta(0) = 1$ only when $x = 0$ and $\delta(x) = 0$ otherwise.

Select the index m according to the term of interest and substitute it into the mask matrix $\mathbf{M}_{(m)}$. This can be expressed as Eqs. (29) and (30), and the resulting form is equivalent to Eq. (14).

$$\tau_{ij}^{p}\left(\theta_k^{(m)}\right) = \begin{bmatrix} c_{0k} & c_{1k} & c_{2k} \end{bmatrix} \boldsymbol{M}_{(m)} \begin{bmatrix} \theta_k \\ \dot{\theta}_k \\ \ddot{\theta}_k \end{bmatrix} \tag{29}$$

$$= c_{mk}\, \theta_k^{(m)} \tag{30}$$

Using a mask matrix, we can identify motion-propagation forces and thereby extract the joint torques attributable to each link's motion. We apply this to the extraction of salient behaviors in construction machinery.

Fig. 1: The computation graph for solving the torque of a one-link robotic arm

C. Salient Behavior Extraction

This section describes a concrete implementation of the proposed formulation. Numerical integration methods for ordinary differential equations, such as the Euler method [8] and Runge–Kutta methods [9], are widely used. The Euler method consists of a single update formula and is computationally simple, but it suffers from relatively large numerical errors. Runge–Kutta methods mitigate this drawback and achieve smaller errors at the cost of additional computations. However, because these approaches rely purely on numerical substitution rather than analytic expressions, further decomposing partial torques to obtain motion-propagation torques leads to high computational cost.

To enable analytic and efficient computation, we employ automatic differentiation. Automatic differentiation (AD) is a technique that analytically computes derivatives of composite functions using a computation graph, in which the computational process is represented by nodes and edges, following a prescribed algorithm. Fig. 1 illustrates the computation graph for solving the torque of a one-link robotic arm using the Lagrangian method.

AD offers two key advantages in this context. First, it is highly compatible with the partial-Lagrangian method. The partial-Lagrangian framework is constructed from energy functions and their derivatives. While deriving the energy terms themselves is straightforward, computing their derivatives becomes difficult for complex models. Because AD handles derivatives of composite functions systematically, combining it with the partial-Lagrangian method allows concise derivation and evaluation of the equations of motion, enabling fast and efficient inverse dynamics analysis. Second, AD preserves analytic expressions. Unlike numerical differentiation, which leaves only numerical values, AD retains the computation graph and thus the intermediate expressions. As a result, joint torques and additional decomposed components, such as motion-propagation torques, can be obtained simultaneously.

By applying this approach, the formulations introduced above can be extracted directly from gradients. Consequently, even in complex equations of motion, arbitrary terms of interest can be selectively analyzed.

III. Experimental Methods

A. Overview of Excavation Experiments with Construction Machinery

To represent the machine's behavior as a robotic arm, we model the excavator as a planar four-link system, as

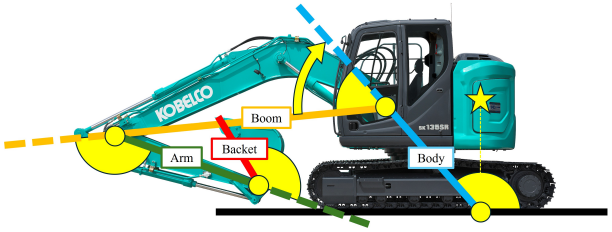

Fig. 2: Planar Four-Link Model of the Construction Machine

shown in Fig. 2. In this study, the model is applied to a Kobelco SK135SR-5 hydraulic excavator. Joint angles are defined positive counterclockwise, while joint torques are defined positive clockwise. Link lengths, moments of inertia, and centers of mass are set with reference to the physical parameters of the actual machine. For Joint 1, the joint location is taken as the ground contact point obtained by vertically projecting the mass center of the base machine with the attachment removed.

Using this excavator, we conducted an excavation task with a single participant. The onboard system measured each joint angle and the magnitude and direction of the force acting on the bucket, while an IMU (DhaibaDAQ, AIST) mounted on the seatback recorded the seat's angular velocity.

The measured signals were processed using a third-order Butterworth low-pass filter, with a passband of 1 Hz and a stopband of 3 Hz. Joint angular velocities/accelerations and seat angular acceleration were then obtained by differentiating the joint angles and seat angular velocity using the nine-point finite-difference formula.

In this experiment, we focus on the torque τ_1 acting on the base (where the seat is located), and, in particular, extract the component of τ_1 generated by the external force at the end effector; we denote this τ_{1ex}.

IV. Results

The results of the visual inspection of the machine's behavior are summarized in TABLE II.

TABLE II: Construction-Machine Operations and Timing

Operations	Time [s]
Ground contact	8∼9, 34∼35
Dumping	27∼28

The forces acting on the bucket are shown in Figs. 3. The upper panel is the horizontal component in the sagittal plane (from the operator's viewpoint), and the lower panel is the vertical component. Red segments indicate periods when the tool tip was below ground level, i.e., during excavation.

The time-domain signals of τ_1 and its external-force component τ_{1ex} and their corresponding frequency distributions, are presented in Figs. 4 and 5, respectively.

These results indicate that isolating τ_{1ex} reduces the spectral intensity; in particular, in the relatively high-frequency band of 2.0–3.0 Hz, the spectral intensity of τ_{1ex} was approximately 70% of that of τ_1.

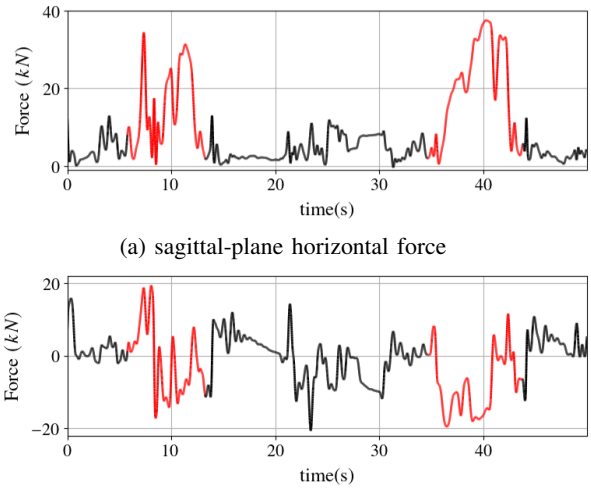

(a) sagittal-plane horizontal force

(b) sagittal-plane vertical force

Fig. 3: End-effector external force components in the sagittal plane

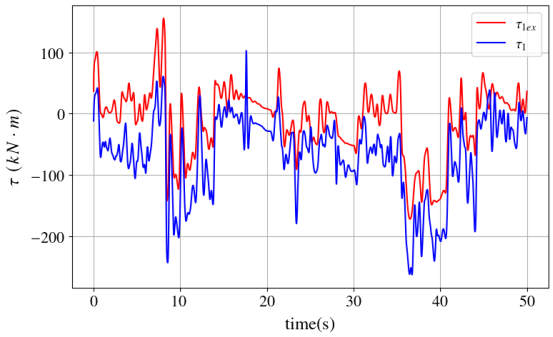

Fig. 4: τ_1 and τ_{1ex} during the experiment

Furthermore, the lumbar load index during this task is shown in Fig. 6. This value was derived based on the system using intervertebral disc compression force proposed by Tsuchiya et al[10].

V. Discussion

Because a correlation between seat vibration and lumbar load in construction machinery has been reported [11], the results in Fig. 5 suggest that selectively extracting per-link motion components for remote-seat vibration rendering reduces unwanted vibrations and may help alleviate lumbar load.

In addition, we compute the band-integration ratio R in the 0–6 Hz range using the amplitudes of τ_1 and $\tau_{1\mathrm{ex}}$. Here, A_1 and $A_{1\mathrm{ex}}$ denote the amplitudes of τ_1 and $\tau_{1\mathrm{ex}}$ at frequency bin f_k, respectively. This yields $R = 0.72$. Using the same procedure for τ_1 with the 4–5 Hz band removed, which corresponds to the human resonance frequency and is regarded as harmful to the human body, gives $R = 0.99$, i.e., almost no change. These results indicate that the proposed motion-equation-based selective vibration presentation on the

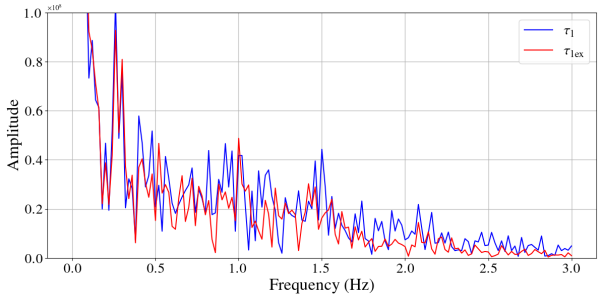

Fig. 5: Frequency spectra of τ_1 and τ_{1ex}

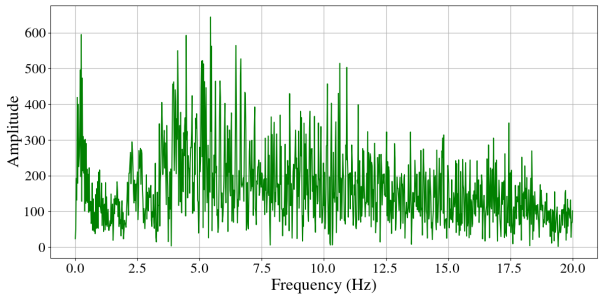

Fig. 7: Frequency spectrum of the seat angular acceleration

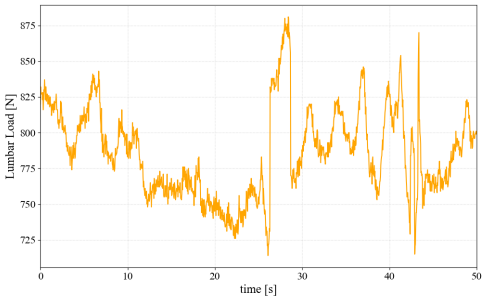

Fig. 6: Lumbar load during the experiment

motion seat, unlike conventional frequency-band separation, provides a more effective means of controlling vibration.

$$R = \frac{\sum_{k\,:\,f_k \in [0,6]} A_{1\mathrm{ex}}[k]}{\sum_{k\,:\,f_k \in [0,6]} A_{\mathrm{all}}[k]} \times 100$$

Next, we demonstrate, via a continuous wavelet transform (CWT)–based similarity analysis, that the salient behaviors extracted by torque decomposition influence seat angular acceleration.

We computed the wavelet transforms of the torque and the seat angular acceleration using the Python library PyWavelets. The continuous wavelet transform (CWT) was performed as in Eq. (31), yielding W_α and W_β for the torque and seat-angular-acceleration signals, respectively.

As the mother wavelet, we used the complex Morlet with bandwidth 1.5 and center frequency 1.0. The sampling period was 5 ms; the scale a ranged from 1 to 256; and the convolution was carried out by time shifts b.

$$W_i(a,b) = \frac{1}{\sqrt{|a|}} \int_{-\infty}^{\infty} x(t)\, \psi^* \left(\frac{t-b}{a} \right) dt \qquad (31)$$

where $\quad i \in \{\alpha, \beta\}$

Subsequently, both signals are min–max normalized as in Eq. (32), and, following Eq. (33), the element-wise product of their CWTs is computed to obtain the time–frequency similarity.

$$W_i{}' = \frac{W_i - W_i\mathrm{min}}{W_i\mathrm{max} - W_i\mathrm{min}} \qquad (32)$$

$$S(a,b) = \left| W_\alpha{}'(a,b) \right| \cdot \left| W_\beta{}'(a,b) \right| \qquad (33)$$

From the result of Eq. (33), we identify the motions with high similarity.

Fig. 7 shows the frequency distributions of the seat angular acceleration. The vertical axis indicates spectral intensity and the horizontal axis indicates frequency. Taken together with Fig. 5, which shows that τ_1 is concentrated below 3Hz, this implies that the influence of τ_1 on seat angular velocity is likewise concentrated below 3Hz.

Based on the above equations and results, Fig. 8 illustrates the procedure for computing the similarity between τ_{1ex} and the seat angular acceleration.

Together with Table 2, it shows that the similarity increases at the same timings as ground contact and soil discharge, indicating that τ_{1ex} influences the seat angular acceleration at those moments.

VI. Conclusion

In this study, we proposed a method for selectively rendering seat angular acceleration during teleoperation of construction machinery by decomposing joint torques and extracting motion-propagation components associated with salient operator-perceived vibrations. By leveraging the partial Lagrangian method and the concept of motion-propagation force, we isolated the torque components generated at the base joint due to specific link motions and demonstrated their influence on seat angular acceleration through wavelet-based similarity analysis.

Experimental validation using a full-scale hydraulic excavator confirmed that these salient torque components correspond to key operational events, such as ground contact and soil discharge, and significantly contribute to the seat's dynamic behavior. These findings suggest that targeted vibration feedback, based on physically interpretable motion elements, can preserve kinesthetic realism while potentially reducing unnecessary whole-body vibrations that contribute to operator fatigue and lumbar load.

This work offers a new perspective for designing haptic feedback systems in teleoperated heavy machinery, where the balance between operational immersion and physical strain is critical. By shifting from naive reproduction of seat motion to selective, physically-grounded vibration synthesis,

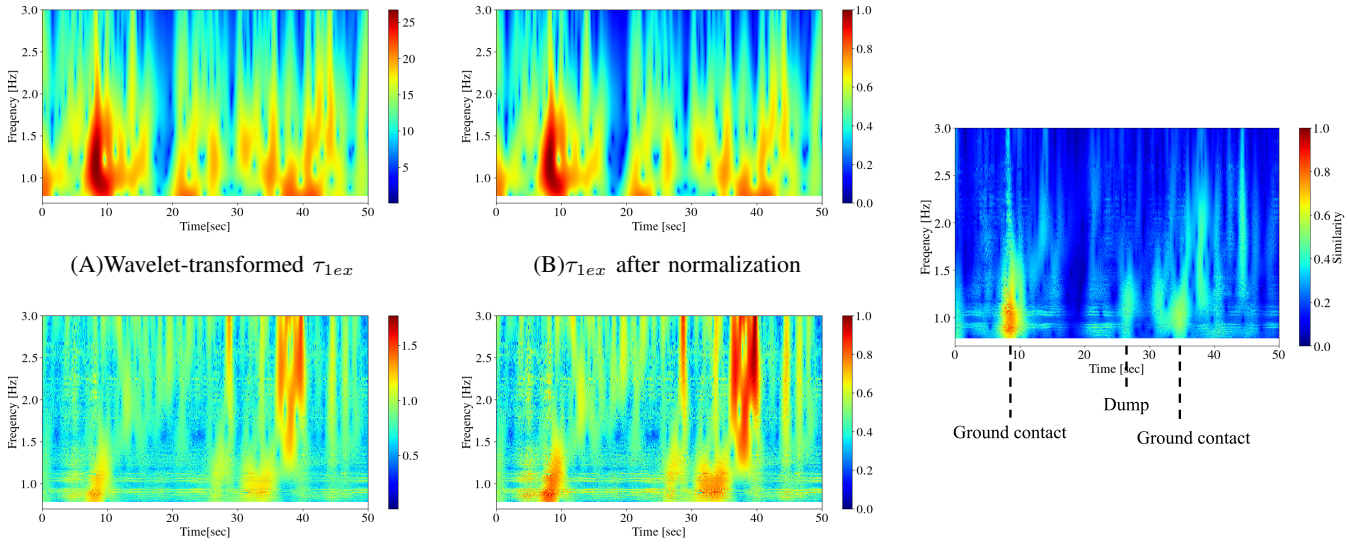

(A)Wavelet-transformed τ_{1ex}

(B)τ_{1ex} after normalization

(A)Wavelet-transformed Seat angular acceleration

(B)Seat angular acceleration after normalization

(C)After cross-correlation and event

Fig. 8: Wavelet transforms and similarity between the external-force term (top) and the seat angular acceleration (bottom)

the proposed method contributes toward more intelligent and ergonomic remote operation systems.

As future work, we plan to conduct user studies to evaluate how the proposed vibration rendering affects subjective perception, operational precision, and physical comfort. In addition, integrating this method with adaptive control platforms may further enhance the personalization and effectiveness of haptic feedback in construction robotics.

REFERENCES

[1] H. Kim, J. Kim, B. An , T. Song, J. Oh, M. Kim, and S. Lee, “ The influence of real-time feedback on excavator operator actions in footing excavation: Machine guidance and conventional methods, ” Appl. Sci., vol. 15, no. 7, p. 3729, 2025.

[2] M. C. S. Meera, P. S. Sairam, V. Veeramalla, A. Kumar, and M. K. Gupta, “ Design and analysis of new haptic joysticks for enhancing operational skills in excavator control, ” J. Mech. Des., vol. 142, no. 12, p. 121406, Dec. 2020.

[3] K. Ahn, “ Development of force reflecting joystick for hydraulic excavator, ” JSME International Journal, vol. 47, no. 3, pp. 858–863, 2004.

[4] Kusaka T, Tanaka T. “ Partial Lagrangian for Efficient Extension and Reconstruction of Multi-DoF Systems and Efficient Analysis Using Automatic Differentiation, ” Robotics, vol. 11 No.6, 149 December 2022.

[5] H. Gunji, T. Kusaka, and T. Tanaka, “ A motion propagation force analysis of multi-DoF systems using the partial Lagrangian method, ” Robotics, vol. 14, no. 5, p. 54, Apr. 2025.

[6] S. A. Kassam and H. V. Poor, “ Robust techniques for signal processing: A survey, ” Proc. IEEE, vol. 73, no. 3, pp. 433–481, Mar. 1985.

[7] J. Morlet and G. Grossmann, “Decomposition of Hardy functions into square - integrable wavelets of constant shape, ” SIAM J. Math. Anal., vol. 15, no. 4, pp. 723 – 736, 1984.

[8] Hahn, G.D. A modified Euler method for dynamic analyses. Int. J. Numer. Methods Eng. 1991, 32, 943–955.

[9] Buthcher, J.C. A history of Runge-Kutta methods. Appl. Numer. Math. 1996, 20, 247–260.

[10] K. Tsuchiya, T. Tanaka, S. Kaneko, and O. Kanai, “ Wearable sensor system for estimating lumbar load, ” Doctoral dissertation, Hokkaido University, Information Science, No. 13090, 2018.

[11] R. Sumiyama, T. Kusaka, Y. Kurita, F. Sakamoto, M. Ito, N. Yumoto, and T. Tanaka, “ Relationship between operator’s lumbar load and seat dynamics in real and teleoperated construction machinery, ” in Proc. 57th SICE Hokkaido Branch Annual Conf., pp. 73–75 Hakodate, Japan, Mar. 2025.